PHYSICAL REVIEW D **96,** 074037 (2017)

Study of spin-dependent structure functions of ^{3}He and ^{3}H at NNLO approximation and corresponding nuclear corrections

Hamzeh Khanpour,[1,2,*] S. Taheri Monfared,[2,†] and S. Atashbar Tehrani[3,‡]

[1]*Department of Physics, University of Science and Technology of Mazandaran, P.O. Box 48518-78195 Behshahr, Iran*

[2]*School of Particles and Accelerators, Institute for Research in Fundamental Sciences (IPM), P.O. Box 19395-5531 Tehran, Iran*

[3]*Independent researcher, P.O. Box 1149-8834413 Tehran, Iran*

(Received 13 July 2017; published 30 October 2017)

We determine polarized parton distribution functions (PPDFs) and structure functions from recent experimental data of polarized deep inelastic scattering (DIS) on nucleons at next-to-next-to-leading order (NNLO) approximation in perturbative quantum chromodynamics (pQCD). The nucleon polarized structure functions are computed using the Jacobi polynomial approach while target mass corrections (TMCs) are included in our fitting procedure. Having extracted the polarized spin structure functions, we extend our study to describe ^{3}He and ^{3}H polarized structure functions, as well as the Bjorken sum rule. We also explore the importance of the nuclear corrections on the polarized nuclear structure functions at small and large values of x. Our results are compared with the recent available and high precision polarized ^{3}He and ^{3}H experimental data.

DOI: 10.1103/PhysRevD.96.074037

I. INTRODUCTION

Precise understanding of parton distribution functions (PDFs) will be a key ingredient in searches for new physics at the LHC through, for example, top-quark and Higgs-boson coupling measurements. Consequently, reliable extraction of information on the unpolarized parton distribution functions (PDFs) [1–5], polarized PDFs (PPDFs) [6–10], and nuclear PDFs [11–14] from global QCD analyses of deep inelastic scattering (DIS) data, as well as many related studies [15–41], provides deep understanding of the hadrons' structure in term of their quarks and gluon constituents.

The determination of the longitudinal spin structure of the nucleon caused a huge growth of interest in polarized DIS experiments after the surprising EMC [42,43] result that the quark spin contribution to the nucleon spin of $1/2$ might be significantly small. In subsequent measurements by SMC [44], it was confirmed that the quark spin contributes about one third of the spin of the nucleon. Many experiments have been conducted at SLAC, DESY, and CERN to extract the nucleon spin-dependent structure functions $g_1(x, Q^2)$ and $g_2(x, Q^2)$. Various analyses of the world data of A_1 or g_1 based on next-to-leading order (NLO) [7–10] and next-to-next-to-leading order (NNLO) [6,45] calculations in perturbative quantum chromodynamics (pQCD) have been carried out to extract the polarized parton densities along with the estimation of their uncertainties.

Previously in TKAA16 [6], we carried out the first pQCD analysis using Jacobi polynomial approach at NNLO approximation based on only $g_1^{p,n,d}(x, Q^2)$ experimental data. In our latest study KTA-I17 [45], we have extended our NNLO formalism by including target mass corrections (TMCs) and Higher twists (HT) terms and enriched it by more data from $g_2^{p,n,d}(x, Q^2)$ observables. In this analysis also the Jacobi polynomials were implemented to determine the polarized parton distribution functions. This method has been applied to various QCD calculations [6,45–49] containing the case of polarized and unpolarized PDF analyses.

In the absence of polarized charged current neutrino experiments, individual light quark sea densities cannot in principle be determined. The inclusive polarized deep inelastic lepton-hadron reactions can only provide information about the $\Delta u + \Delta\bar{u}$, $\Delta d + \Delta\bar{d}$, and $\Delta s + \Delta\bar{s}$, along with the gluon. For many years our group [6,45,50], LSS [51,52], BB10 [53], and other people made simplifying assumptions about the sea quark densities and consequently were able to present results for the valence u_v and d_v. In the present study, we applied all polarized g_1 data, including very recent COMPASS16 g_1^p and g_1^d data [54,55], to determine the sum of quark and antiquark polarized PDFs $\Delta q(x) + \Delta\bar{q}(x)$. This method provides no information about the individual polarized quark and antiquark distributions. We focused only on g_1 experimental data due to their smaller uncertainties compared with the g_2 measurements, indicating the lack of knowledge in the g_2 structure function. Before one can precisely extract PPDF, it is important to take into account the target mass corrections arising from purely kinematic effects.

*Hamzeh.Khanpour@mail.ipm.ir
†Sara.Taheri@ipm.ir
‡Atashbart@gmail.com

In addition to the scattering of polarized lepton beams from a polarized nucleon, the polarized light nuclear targets provided the opportunity to probe the spin structure of the nucleon. Among these are the SMC experiments at CERN [44] and the E143 [56] and E155 [57] experiments at SLAC that used polarized deuterium. Meanwhile, the HERMES Collaboration at DESY [58] and the E154 experiments at SLAC [59,60] utilized polarized ^{3}He. Recently both polarized ^{3}He and ^{3}H targets were used at E06-014 experiments at Jefferson Lab (JLAB) in Hall A, which are the latest and most up-to-date data for the spin-dependent g_1 and g_2 structure functions of ^{3}He [61]. Hence, we step further from the "structure of nucleon" to "nuclei" in terms of their parton constituents. In order to study the polarized nuclear structure function, $g^A_{1,2}(x, Q^2)$, one needs to consider nuclear corrections. In this paper, we study the nuclear effects in inclusive scattering of polarized leptons from polarized ^{3}He and ^{3}H nuclei in the DIS region. We focus in particular on kinematics at intermediate and large values of x where the major contributions come from the incoherent scattering.

This paper is organized as follows. In Sec. II, we provide an overview of data sets. In Sec. III, we review our theoretical framework and summarize the basic formulas relevant for the analysis. Section IV contains the formalism used for computing the χ^2 minimization and PPDF uncertainties. We introduce the nuclear structure functions and corresponding nuclear corrections in Sec. V. In Sec. VI we discuss how well the predictions for the NNLO analysis and the inclusion of TMCs effects into NNLO polarized structure function analysis improves the precision of the extracted PPDFs as well as nuclear structure functions. Finally, in Sec. VII we summarize our findings.

II. OVERVIEW OF DATA SETS

The combined set of data was included in our NNLO QCD fit to the available g_1^p, g_1^n, and g_1^d world data. For the proton data we use E143 [56], HERMES98 [62], HERMES06 [63], SMC [44], EMC [42,43], E155 [64], COMPASS10 [65], and COMPASS16 [55]; for the neutron data we use E142 [66], E154 [67], HERMES98 [62], HERMES06 [58], JLAB03 [68], JLAB04 [69], and JLAB05 [70]; and for the deuteron data we use E143 [56], E155 [57], SMC [44], HERMES06 [63], COMPASS05 [71], COMPASS06 [72], and COMPASS16 [54]. These data sets are summarized in Table I.

The x and Q^2 nominal coverage of the data considered in our QCD fit is illustrated in Fig. 1. This plot nicely

TABLE I. Summary of published polarized DIS experimental data points with measured x and Q^2 ranges and the number of data points, the χ^2 for each given data set, and the fitted normalization shifts $\mathcal{N}_i$.

Experiment	Ref.	$[x_{\min}, x_{\max}]$	Q^2 range (GeV^2)	Number of data points	χ^2	$\mathcal{N}_n$
E143(p)	[56]	[0.031–0.749]	1.27–9.52	28	21.424	1.00034601
HERMES(p)	[62]	[0.028–0.66]	1.01–7.36	39	75.369	1.00186515
SMC(p)	[44]	[0.005–0.480]	1.30–58.0	12	10.803	0.99991146
EMC(p)	[42]	[0.015–0.466]	3.50–29.5	10	3.328	1.00220752
E155	[64]	[0.015–0.750]	1.22–34.72	24	35.170	1.024762208
HERMES06(p)	[63]	[0.026–0.731]	1.12–14.29	51	22.672	1.00018245
COMPASS10(p)	[65]	[0.005–0.568]	1.10–62.10	15	26.670	0.99301000
COMPASS16(p)	[55]	[0.0035–0.575]	1.03–96.1	54	53.912	1.00019414
g_1^p				**233**		
E143(d)	[56]	[0.031–0.749]	1.27–9.52	28	38.159	0.99916419
E155(d)	[57]	[0.015–0.750]	1.22–34.79	24	18.871	0.99991576
SMC(d)	[44]	[0.005–0.479]	1.30–54.80	12	18.375	0.99998812
HERMES06(d)	[63]	[]0.026–0.731]	1.12–14.29	51	47.045	1.00001347
COMPASS05(d)	[71]	[0.0051–0.4740]	1.18–47.5	11	8.490	0.99692499
COMPASS06(d)	[72]	[0.0046–0.566]	1.10–55.3	15	12.874	0.99991619
COMPASS16(d)	[54]	[0.0045–0.569]	1.03–74.1	43	37.297	1.00089129
g_1^d				**184**		
E142(n)	[66]	[0.035–0.466]	1.10–5.50	8	7.466	0.99899932
HERMES(n)	[62]	[0.033–0.464]	1.22–5.25	9	2.697	0.99995848
E154(n)	[67]	[0.017–0.564]	1.20–15.00	17	9.216	0.99961961
HERMES06(n)	[58]	[0.026–0.731]	1.12–14.29	51	17.974	1.00001347
Jlab03(n)	[68]	]0.14–0.22]	1.09–1.46	4	0.0469	0.99981391
Jlab04(n)	[69]	[0.33–0.60]	2.71–4.8	3	3.651	0.90000096
Jlab05(n)	[70]	[0.19–0.20]	1.13–1.34	2	1.674	1.02232189
g_1^n				**94**		
Total			**511**		**473.195**	

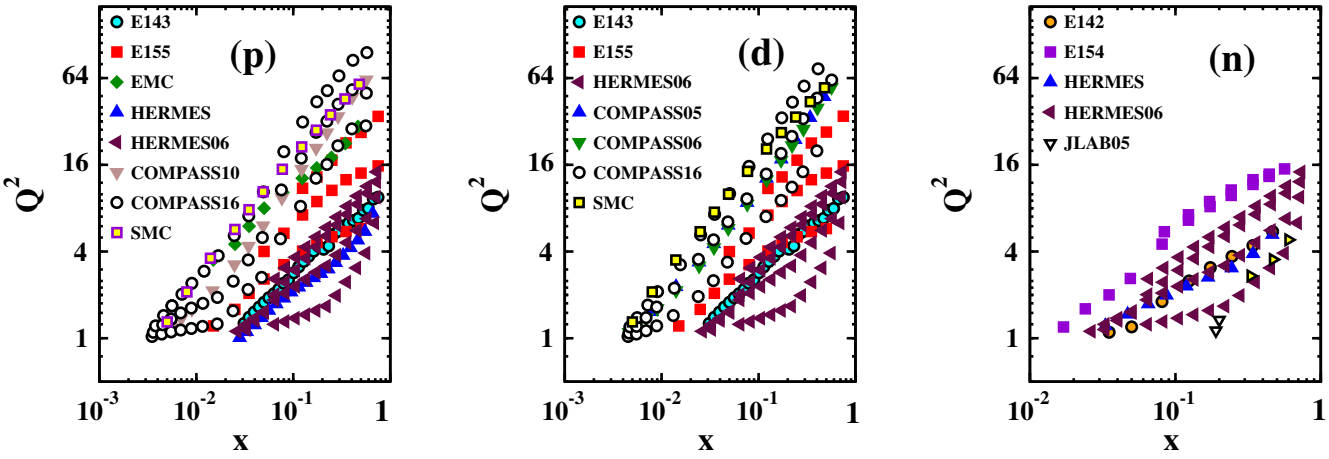

FIG. 1. Nominal coverage of the data sets used in the KTA-II17 analysis for proton, neutron, and deuteron observables. DIS data are presented on a logarithmic x and Q^2 scales.

represents the kinematic coverage of x, and Q^2 of the proton, neutron, and deuteron polarized structure functions. Recent COMPASS results for protons and deuterons [54,55] at low x ($x < 0.03$) increase considerably the accuracy compared to the only available result in this region, SMC [44]. Despite recent outstanding experimental efforts, the kinematical coverage of present polarized DIS observables is still rather limited. Our data (511 experimental data points) cover the kinematic range $0.0035 < x < 0.75$, $1\,(\mathrm{GeV}^2) < Q^2 < 100\,(\mathrm{GeV}^2)$, and $W > 4$ GeV.

This coverage leads to wider uncertainty for extracted polarized PDFs at small x. Consequently, the polarized gluon distribution $\Delta G(x, Q^2)$ and strange distribution $(\Delta s + \Delta\bar{s})(x, Q^2)$ are still weakly constrained, especially for the case of the polarized gluon distribution. Any conclusion on gluon treatment at $x < 0.01$ relies on the behavior of low x polarized DIS data, which is not accurately known up to now. The statistical and systematic uncertainties are both taken into account. The systematic uncertainties are added quadratically.

III. THEORETICAL ANALYSIS

A. Leading-twist polarized DIS structure functions

The calculations applied in this analysis are all performed at NNLO approximation. Correspondingly, the polarized PDFs evolve from the input scale Q_0^2 using NNLO splitting functions [73] and the NNLO hard scattering cross section expressions are considered. To have a full leading-twist (LT) analysis we shall write

$$g_{1,2}(x, Q^2)_{\mathrm{LT}} = g_{1,2}(x, Q^2)_{\mathrm{pQCD}} + h_{1,2}^{\mathrm{TMCs}}(x, Q^2)/Q^2, \quad (1)$$

where $h_{1,2}^{\mathrm{TMCs}}(x, Q^2)$ is explained in Sec. III B. The NNLO spin-dependent proton structure functions, $g_1^{\mathrm{p}}(x, Q^2)_{\mathrm{pQCD}}$, can be written as a linear combination of polarized parton distribution functions Δq, $\Delta\bar{q}$, and Δg as

$$g_1^{\mathrm{p}}(x, Q^2)_{\mathrm{pQCD}} = \frac{1}{2}\sum_q e_q^2 \Delta q_{\mathrm{NS}}(x, Q^2) \otimes \left(1 + \frac{\alpha_s(Q^2)}{2\pi}\Delta C_q^{(1)} + \left(\frac{\alpha_s(Q^2)}{2\pi}\right)^2 \Delta C_{\mathrm{NS}}^{(2)}\right) + e_q^2(\Delta q + \Delta\bar{q})(x, Q^2)$$
$$\otimes \left(1 + \frac{\alpha_s(Q^2)}{2\pi}\Delta C_q^{(1)} + \left(\frac{\alpha_s(Q^2)}{2\pi}\right)^2 \Delta C_s^{(2)}\right) + \frac{2}{9}\left(\frac{\alpha_s(Q^2)}{2\pi}\Delta C_g^{(1)} + \left(\frac{\alpha_s(Q^2)}{2\pi}\right)^2 \Delta C_g^{(2)}\right) \otimes \Delta g(x, Q^2), \quad (2)$$

where the ΔC_q and ΔC_g are the spin-dependent quark and gluon hard scattering coefficient functions, calculable at NNLO approximation [74,75]. The symbol $\otimes$ represents the typical convolution in Bjorken x space. Considering the polarized proton structure function, we can apply isospin symmetry to achieve the neutron one. The deuteron structure function is related to that of the proton and neutron via

$$g_1^{\mathrm{d}}(x, Q^2)_{\mathrm{LT}} = \frac{1}{2}\{g_1^{\mathrm{p}}(x, Q^2)_{\mathrm{LT}} + g_1^{\mathrm{n}}(x, Q^2)_{\mathrm{LT}}\} \times (1 - 1.5 w_D), \quad (3)$$

where $w_D = 0.05 \pm 0.01$ is the probability to find the deuteron in a D-state [76–78].

One can use the Wandzura and Wilczek (WW) [61,79] approximation for the leading-twist g_2 polarized structure function

$$g_2(x,Q^2)_{\mathrm{pQCD}} = g_2^{WW}(x,Q^2) = -g_1(x,Q^2)_{\mathrm{pQCD}} + \int_x^1 \frac{dy}{y} g_1(y,Q^2)_{\mathrm{pQCD}}. \quad (4)$$

Target mass corrections do not affect the WW relation if all powers in (M^2/Q^2) are included [79].

B. Target mass corrections

As illustrated in Fig. 1, in polarized DIS most of the small x experimental data points are at low Q^2, which is one of the features of polarized DIS. In the unpolarized case we can cut the preasymptotic region data, while it is impossible to perform such a procedure for present data on spin-dependent structure functions without losing too much information. To perform a reliable QCD fit including data at lower Q^2 values, target mass corrections cannot be ignored. The standard approach to calculate TMCs in the case of unpolarized DIS is the one based on the operator product expansion (OPE) in QCD, first formulated by Georgi and Politzer [80]. This closed-form expression is generalized in Ref. [81].

We have performed an analysis to higher terms in the TMC expansion based on the method of Ref. [8] and found that these terms do not change the agreement with g_1 data and the extracted polarized parton densities are insensitive to such a choice. We claim that leading terms in the TMC expansion are reliable in the kinematical range of presently available g_1 data. In our previous study, KTA-I17 [45], we presented the significant effect of considering TMCs and HT contributions while g_2 structure function data are included.

To consider the full LT approach [Eq. (1)] in our analysis, we applied the method suggested in Refs. [82–84]. This method effectively depends on the LT term (for more details, see our paper [45]). For simplicity of notation, from now to the end of the paper, we will drop the subscript "LT" denoting the leading twist.

C. PDF parametrizations and conventions

The method applied to reconstruct the x-dependent quantities from their Mellin moments is the Jacobi polynomial method (the same as our previous QCD analyses [6,45]). The main difference, as indicated in Sec. I, is that we consider a new input parametrization at the initial scale $Q_0^2 = 1\ \mathrm{GeV}^2$ for the sum of quark and antiquark polarized PDF instead of the valence and sea distributions, which are more general. We consider the general form of

$$\begin{aligned}
x(\Delta u + \Delta\bar{u})(x,Q_0^2) &= \eta_{u_+} A_{u_+} x^{\alpha_{u_+}} (1-x)^{\beta_{u_+}} \times (1 + \epsilon_{u_+}\sqrt{x} + \gamma_{u_+} x),\\
x(\Delta d + \Delta\bar{d})(x,Q_0^2) &= \eta_{d_+} A_{d_+} x^{\alpha_{d_+}} (1-x)^{\beta_{d_+}} (1 + \gamma_{d_+} x),\\
x(\Delta s + \Delta\bar{s})(x,Q_0^2) &= \eta_{s_+} A_{s_+} x^{\alpha_{s_+}} (1-x)^{\beta_{s_+}},\\
x\Delta G(x,Q_0^2) &= \eta_G A_G x^{\alpha_G} (1-x)^{\beta_G} \times (1 + \epsilon_G\sqrt{x} + \gamma_G x). \quad (5)
\end{aligned}$$

Here, the notation $q_+ = q + \bar{q}$ is applied for light quarks. The normalization factors, A_i, are fixed such that η_i represent the first moments of the polarized distributions. As usual, the set of free parameters in Eq. (5) is constrained by the well-known sum rules

$$\begin{aligned}
a_3 &= g_A = \mathrm{F} + \mathrm{D} = 1.269 \pm 0.003,\\
a_8 &= 3\mathrm{F} - \mathrm{D} = 0.585 \pm 0.025. \quad (6)
\end{aligned}$$

Here, a_3 and a_8 are nonsinglet combinations of the first moments of the polarized parton distributions corresponding to the axial charges for octet baryons [85,86]. These parameters, F and D, are measured in hyperon and neutron β decay and finally lead to the constraints

$$\begin{aligned}
a_3 &= (\Delta u + \Delta\bar{u})(Q^2) - (\Delta d + \Delta\bar{d})(Q^2),\\
a_8 &= (\Delta u + \Delta\bar{u})(Q^2) + (\Delta d + \Delta\bar{d})(Q^2)\\
&\quad - 2(\Delta s + \Delta\bar{s})(Q^2). \quad (7)
\end{aligned}$$

So considering Eqs. (6) and (7), the parameters η_{u_+} and η_{d_+} can be extracted versus $\Delta u + \Delta\bar{u}$, $\Delta d + \Delta\bar{d}$, and $\Delta s + \Delta\bar{s}$. Here, we do not make any simplifying assumptions on the equality of the light sea quark distributions.

In our previous papers [6,45], we have considered the Jacobi polynomial method to yield the structure functions from their Mellin moments in N space. In the polynomial approach, one can easily expand the polarized structure functions in terms of the Jacobi polynomials $\Theta_n^{\alpha,\beta}(x)$ as follows:

$$xg_1(x,Q^2) = x^\beta (1-x)^\alpha \sum_{n=0}^{N_{\max}} a_n(Q^2)\Theta_n^{\alpha,\beta}(x). \quad (8)$$

Here, $\Theta_n^{\alpha,\beta}(x) = \sum_{j=0}^n c_j^{(n)}(\alpha,\beta)x^j$ and $N_{\max}$ is the maximum order of the expansion. The Jacobi polynomials $\Theta_n^{\alpha,\beta}(x)$ are a class of classical orthogonal polynomials. They are orthogonal with respect to the weight $x^\beta(1-x)^\alpha$

on the interval [0, 1]. In the polynomial approach, the Q^2 dependence of the $xg_1(x,Q^2)$ are codified in the Jacobi polynomial moments, $a_n(Q^2)$. Using the orthogonality relation, one can obtain this moment as

$$a_n(Q^2) = \int_0^1 dx x g_1(x,Q^2)\Theta_n^{\alpha,\beta}(x) = \sum_{j=0}^{n} c_j^{(n)}(\alpha,\beta)\mathcal{M}[xg_1, j+2](Q^2). \quad (9)$$

The Mellin transform $\mathcal{M}[xg_1^{\tau 2}, \mathrm{N}]$ is defined via

$$\mathcal{M}[xg_1, \mathrm{N}](Q^2) \equiv \int_0^1 dx x^{\mathrm{N}-2} xg_1(x,Q^2). \quad (10)$$

Applying the Jacobi polynomial expansion method, the polarized structure function $xg_1(x,Q^2)$ can be constructed as

$$xg_1(x,Q^2) = x^\beta(1-x)^\alpha \sum_{n=0}^{N_{\max}} \Theta_n^{\alpha,\beta}(x) \times \sum_{j=0}^{n} c_j^{(n)}(\alpha,\beta)\mathcal{M}[xg_1, j+2](Q^2). \quad (11)$$

We also scrutinized the sensitivity of the Jacobi polynomials to its free parameters. These results are discussed in detail in Ref. [45]. In our current analysis by setting the $\{N_{\max}=7, \alpha=3, \beta=0.5\}$, the optimal convergence of this expansion throughout the whole kinematic region covered by the polarized DIS data is achievable.

IV. χ^2 MINIMIZATION AND UNCERTAINTIES OF PHYSICAL PREDICTIONS

The goodness of fit is traditionally determined by the effective global χ^2 minimization algorithm that measures the quality of fit between theory and experiment. χ^2_{global} is defined by

$$\chi^2_{\mathrm{global}} = \sum_{i=1}^{N_n^{\mathrm{data}}} w_n \left[\left(\frac{1-\mathcal{N}_n}{\Delta\mathcal{N}_n} \right)^2 + \sum_{i=1}^{N_n^{\mathrm{data}}} \left(\frac{\mathcal{N}_n g_{1,i}^{\mathrm{Exp}} - g_{1,i}^{\mathrm{Theory}}}{\mathcal{N}_n \Delta g_{1,i}^{\mathrm{Exp}}} \right)^2 \right], \quad (12)$$

where n labels the number of different experiments and w_n is a weight factor for the nth experiment. g^{Exp}, Δg^{Exp}, and g^{Theory} indicate the data value, the uncertainty, and the theory value for the data point i of data set n, respectively. The $\Delta\mathcal{N}_n$ are the experimental normalization uncertainty quoted by the experiments. The relative normalization factors, $\mathcal{N}_n$, appear as free parameters in the fit. These 22 normalization shifts are determined at the prefitting procedure along with the PDF free parameters and strong coupling constant using the CERN program library MINUIT [87]. Afterwards, they are fixed at their best fitted values to further reduce the free parameters. Finally, we minimize the above χ^2 value with 16 free parameters, including the strong coupling constant.

To visually evaluate the fit quality, in Fig. 2 we plot the χ^2/dof for individual experiments per nucleon target. This allows us to check that the majority of experiments have a $(\chi^2/\mathrm{dof}) \simeq 1$. It means that most of the experiments satisfy this goodness-of-fit scale parameter. The largest contribution to χ^2 arises from the HERMES and COMPASS10 data for protons, and the SMC data for deuteron structure functions. The smallest contribution comes from the JLAB03 data for xg_1^n. From Fig. 2, one can conclude that the HERMES98 and COMPASS10 data for xg_1^p are difficult to describe based on our fitting scenario. The motivation of considering them in our analysis originates mainly from our goal to have the most complete and up-to-date sets of data for the polarized structure functions.

Different methods to estimate the uncertainties of PDFs obtained from global χ^2 optimization, together with technical details, were described in Refs. [4,11,88–91]. The most common and effective approach is the "Hessian method." In this section the outline of this method is explained because it is used in our analysis. Up to the leading quadratic terms, the χ^2 can be written in terms of the Hessian matrix

$$H_{ij} \equiv \frac{1}{2}\frac{\partial^2\chi^2}{\partial a_i \partial a_j}\bigg|_{\min} \quad (13)$$

as

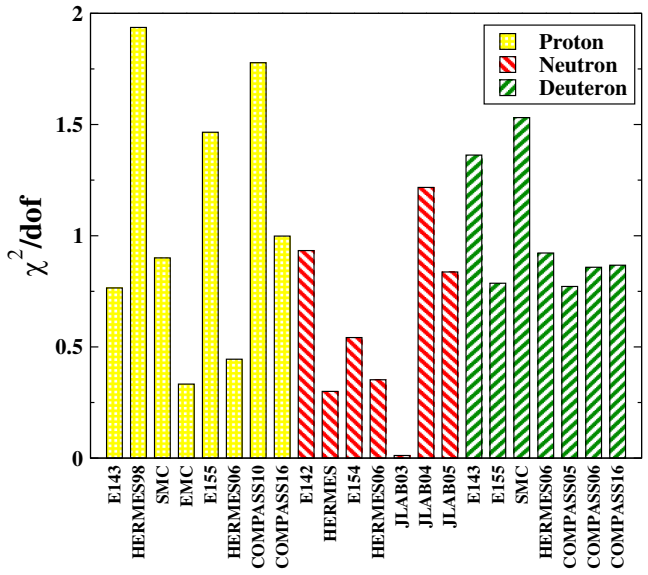

FIG. 2. Value of χ^2/dof for individual experiments per nucleon target used in the KTA-II17.

$$\Delta\chi^2_{\text{global}} = \chi^2_{\text{global}} - \chi^2_{\text{min}} = \sum_{ij}^{N_{\text{par}}} H_{ij}\left(a_i - a_i^{(0)}\right)\left(a_j - a_j^{(0)}\right), \tag{14}$$

where a_i $(i = 1, 2, ..., \text{N})$ refers to the free parameters for each PDF presented in Eq. (5) and N is the number of parameters. $\Delta\chi^2_{\text{global}}$ illustrates the allowed variation in χ^2. The standard formula for linear error propagation is

$$(\Delta q)^2 = \Delta\chi^2_{\text{global}} \sum_{i,j} \frac{\partial \Delta q}{\partial a_i} (H_{ij})^{-1} \frac{\partial \Delta q}{\partial a_j}. \tag{15}$$

The parameter value of polarized PDF, i.e., $a_1^0, \ldots, a_n^0$, extracted from the NNLO QCD fit, will be presented in Sec. VI. Equation (15) is not convenient to use since the derivative of Δq with respect to each parameter a_i is required. An improved iterative method has been devised in [4,88,89] in which the Hessian matrix is diagonalized. We adopt this improved Hessian method in our analysis and work in terms of rescaled eigenvectors and eigenvalues. The PDF uncertainty determination becomes much easier in terms of the appropriately normalized eigenvectors, z_i:

$$\Delta\chi^2_{\text{global}} = \sum_{i}^{N_{\text{par}}} z_i^2. \tag{16}$$

The uncertainty of an individual PDF at particular values of x and Q^2 can be estimated using

$$\Delta q = \Delta\chi^2_{\text{global}} \frac{1}{2} \sqrt{\sum_{k=1}^{n} [\Delta q(S_k^+) - \Delta q(S_k^-)]^2}. \tag{17}$$

Here, S_k^+ and S_k^- are polarized PDF sets displaced along eigenvector directions by the extracted $\Delta\chi^2_{\text{global}}$ value.

With the standard "parameter-fitting" criterion, we would expect the uncertainties to be given by the choice of tolerance parameter $T^2 = \Delta\chi^2_{\text{global}} = 1$ for the 68% (one-sigma-error) confidence level (C.L.) limit [4,89]. For the general case with N degrees of freedom, the $\Delta\chi^2_{\text{global}}$ value needs to be calculated to determine the size of the uncertainties. Assuming that $\Delta\chi^2_{\text{global}}$ follows the χ^2 distribution with N degrees of freedom, we have the C.L. P as [4,89,92]

$$P = \int_0^{\Delta\chi^2_{\text{global}}} \frac{1}{2\Gamma(\text{N}/2)(\frac{S}{2})^{(\text{N}/2)-1}} e^{-\frac{S}{2}} dS. \tag{18}$$

In the case of the one-free-parameter fit, one obviously has $\Delta\chi^2_{\text{global}} = 1$. Since the polarized parton distributions in common QCD fits are considered with several free parameters, $N > 1$, the value of $\Delta\chi^2_{\text{global}}$ should be reevaluated form Eq. (18). Here we calculate the uncertainties of polarized PDFs with $\Delta\chi^2_{\text{global}} = 1$. For other values of $\Delta\chi^2_{\text{global}}$, one can simply scale our error bands by $(\Delta\chi^2_{\text{global}})^{1/2}$.

V. POLARIZED STRUCTURE FUNCTIONS FOR NUCLEI

The experimental data on deep inelastic lepton-nucleus scattering can reveal more information on the behavior of nucleon structure functions and nucleon correlations in nuclei at small and large values of x. This provides a more reliable picture of the nuclear phenomena. Moreover, the absence of free neutron targets means that polarized light nuclei such as deuterium and ^{3}He must be used as effective polarized neutron targets. The scattering of polarized lepton beams from polarized nuclear targets paves the way to study the spin structure of the nucleon encoded in the spin structure functions of g_1 and g_2. In order to extract these spin structure functions from the spin-dependent DIS data on nuclear targets, one needs to account for the nontrivial nuclear effects. The nuclear effects that play an important role in the polarized and unpolarized DIS on nuclei can be divided into coherent and incoherent contributions [93,94]. Incoherent nuclear effects, which are present at all values of x, arise from the scattering of the incoming lepton on each individual nucleon. Some examples of incoherent nuclear effects are Fermi motion, spin depolarizations, binding, and the presence of a non-nucleonic degree of freedom.

The coherent nuclear effects are typically important at low values of the momentum fraction x. They result from the interaction of the incoming lepton with two or more nucleons in the target. Nuclear shadowing, which is important for the region $10^{-4} \leq x \leq 0.03$–0.07, and nuclear antishadowing at 0.03–$0.07 \leq x \leq 0.2$ are examples of the coherent nuclear effects. Nuclear shadowing corrections in polarized ^{3}He have been argued in Refs. [95,96]. These effects arise from multiple scattering of the lepton from two or more nucleons in the ^{3}He nucleus. In addition, contributions to the polarized ^{3}He structure function from non-nucleonic degrees of freedom in the nucleus have been discussed in detail in Refs. [93,94].

For the case of the polarized DIS in which we present in the following analysis, the major contributions come from the incoherent scattering on the nucleons of the target. The aim of this work is to study these nuclear effects for the case of the polarized DIS at NNLO approximation and assess their importance on the spin structure functions of $g_{1,2}^{^3\text{He}}$ and $g_1^{^3\text{H}}$.

In the following, we describe the nuclear effects in inclusive scattering of polarized leptons from polarized helium ^{3}He and tritium ^{3}H nuclei, focusing in particular on kinematics at whole values of momentum fraction x.

A. Weak binding approximation

To begin our discussion on the nuclear corrections, we should note that in the standard nuclear structure function analyses, the contributions from spin depolarization, Fermi motion, and binding are described within the framework of the convolution approach. The polarized nuclear structure function of ^{3}He and ^{3}H can be written as a convolution of the light-cone momentum distributions with the off-shell polarized nucleon structure functions of the proton g_1^p and neutron g_1^n. In what follows, we apply the method presented in Refs. [93,97] and adopt the approach in which the light-cone nucleon momentum distributions can be obtained from the nuclear spectral function [98,99].

The coherent effects associated with the multiple scattering from two or more nucleons in the nucleus give rise to corrections at small values of x. In order to study the nuclear effects in incoherent scattering, we restrict ourselves to the intermediate and large region of momentum fraction x in which the incoherent scattering from a single nucleon is expected to dominate [18,97,100,101]. In this framework, in which the nucleus is treated as a nonrelativistic system of weakly bound nucleons, the spin-dependent structure functions of ^{3}He can be obtained as [102–107]

$$g_1^{^3\mathrm{He}}(x,Q^2) = \int \frac{dy}{y}\left[2\Delta f^p(y,\gamma) g_1^p\left(\frac{x}{y},Q^2\right) + \Delta f^n(y,\gamma) g_1^n\left(\frac{x}{y},Q^2\right)\right], \tag{19}$$

where $y = \frac{p.q}{M\nu}$ is the nuclear light-cone momentum fraction carried by the interacting nucleons. The functions $f^{N(=p,n)}(y,\gamma)$ are nucleon light-cone momentum distributions in the ^{3}He nucleus computed in terms of the nuclear spectral function [93,97]

$$\Delta f^N(y,\gamma) = \int \frac{d^4p}{(2\pi)^4} D^N(\varepsilon,p,\gamma)\delta\left(y-1-\frac{\varepsilon+\gamma p_z}{M}\right), \tag{20}$$

with $N = p$ or n, and D^N is the energy-momentum distribution functions. In the Bjorken limit $(\gamma \to 1)$, the nucleon light-cone momentum distributions $f^N(y,\gamma)$ depend only on y, which spans the range between x and $\frac{M_{^3\mathrm{He}}}{M} \approx 3$. Finally, the polarized structure functions of $g_1^{^3\mathrm{He}}$ and $g_1^{^3\mathrm{H}}$ can be written as

$$g_1^{^3\mathrm{He}}(x,Q^2) = \int_x^3 \frac{dy}{y}\Delta f^n_{^3\mathrm{He}}(y) g_1^n(x/y,Q^2) + 2\int_x^3 \frac{dy}{y}\Delta f^p_{^3\mathrm{He}}(y) g_1^p(x/y,Q^2), \tag{21}$$

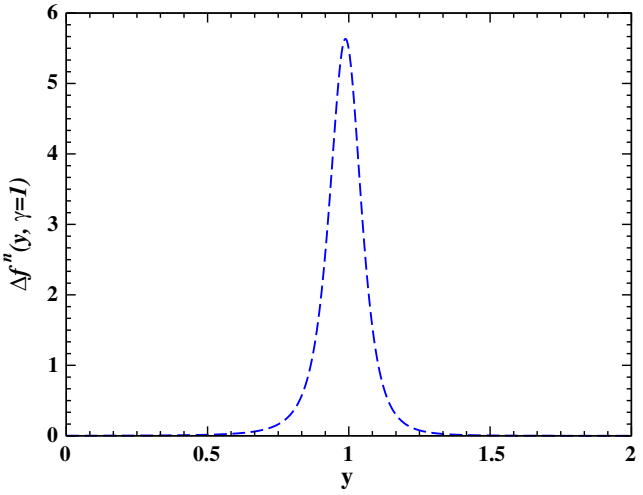

FIG. 3. The polarized neutron light-cone momentum distribution functions at the Bjorken limit $(\gamma \to 1)$ in ^{3}He, based on the results of Ref. [98].

$$g_1^{^3\mathrm{H}}(x,Q^2) = 2\int_x^3 \frac{dy}{y}\Delta f^n_{^3\mathrm{H}}(y) g_1^n(x/y,Q^2) + \int_x^3 \frac{dy}{y}\Delta f^p_{^3\mathrm{H}}(y) g_1^p(x/y,Q^2). \tag{22}$$

The Fermi motion and their binding are parametrized through the distributions $\Delta f^{N(=p,n)}_{^3\mathrm{He}}$ and $\Delta f^{N(=p,n)}_{^3\mathrm{H}}$, which can be calculated using the ground-state wave functions of ^{3}He and ^{3}H nuclei. It is worth mentioning that, because of isospin symmetry, the light-cone momentum distribution $\Delta f^p_{^3\mathrm{He}}(y)$ is equal to $\Delta f^n_{^3\mathrm{H}}(y)$.

To obtain the polarized light-cone momentum distributions we used the numerical results of Ref. [98]. The polarized light-cone distribution functions for the neutron $\Delta f^n_{^3\mathrm{He}}(y)$ and proton $\Delta f^p_{^3\mathrm{He}}(y)$ are shown as a function of y in Figs. 3 and 4, respectively. It has been shown in various studies that the polarized light-cone distribution functions $\Delta f^N(y,\gamma=1)$ are sharply peaked at $y \approx 1$ [98,99,105].

B. Effective polarizations of the nucleons

In the limit of zero nuclear binding and the Bjorken limit $(\gamma \to 1)$, the polarized proton light-cone momentum distribution functions $\Delta f^N(y)$ become infinitesimally narrow and are sharply peaked around $y \approx 1$ $\{f^N \sim \delta(1-y)\}$, due to the small average separation energy per nucleon. Thus, in this approximation, one can express the polarized nuclear structure functions $g_1^A(x,Q^2)$ as linear combinations of the polarized proton g_1^p and neutron g_1^n structure functions weighted by effective polarizations. Consequently, Eq. (19) is often approximated by

$$g_1^{^3\mathrm{He}}(x,Q^2) = 2P^p g_1^p(x,Q^2) + P^n g_1^n(x,Q^2). \tag{23}$$

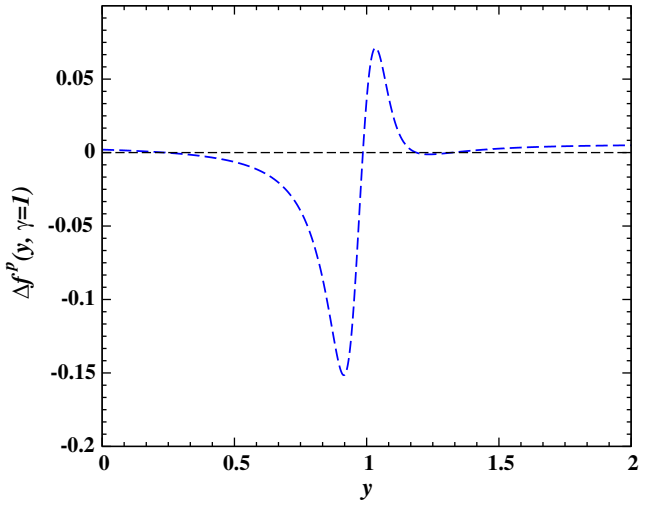

FIG. 4. The polarized proton light-cone momentum distribution functions at the Bjorken limit ($\gamma \to 1$) in ^{3}He, based on the results of Ref. [98].

Here P^p and P^n are the proton and neutron effective polarizations inside the polarized ^{3}He nucleus. The proton effective polarizations P^p are assumed to be the average polarizations of the two protons in ^{3}He. The effective polarizations are described in terms of integrals of the diagonal light-cone momentum distribution functions at the Bjorken limit ($\gamma \to 1$) as

$$P^p = \int_0^3 dy \Delta f^p_{^3\mathrm{He}}(y, \gamma = 1),$$
$$P^n = \int_0^3 dy \Delta f^n_{^3\mathrm{He}}(y, \gamma = 1). \quad (24)$$

The effective polarizations can be computed numerically from models of the ^{3}He nucleus wave function. The calculations of Refs. [98,108] have shown that $P^p = -0.028 \pm 0.004$ and $P^n = 0.86 \pm 0.02$.

C. Non-nucleonic contributions

As we have discussed earlier, the free nucleons behave differently from those bound in nuclei. This is due to nuclear corrections such as nuclear binding, Fermi motion, nuclear shadowing, and antishadowing, as well as non-nucleonic degrees of freedom. Consequently, the description of the nucleon as a mere collection of protons and neutrons (i.e., a description of nuclear properties in terms of nucleon degrees of freedom alone) may not be complete and hence the nuclear corrections due to non-nucleonic degrees of freedom need to be considered. For the spin-dependent observables $g_1^A(x, Q^2)$, a small admixture of the $\Delta(1232)$ isobar in the three-body wave function was found to be necessary for a better description of the polarized nuclear structure functions [109]. In order to consider nuclear effects that originate from non-nucleonic degrees of freedom, we utilized the work presented in Ref. [93], which provides a description of the $g_1(x, Q^2)$ spin structure functions of helium ^{3}He and tritium ^{3}H nuclei over the range of $10^{-4} \le x \le 0.8$. It models the ^{3}He wave function, including the S, S', and D states and the non-nucleonic degrees of freedom from the $\Delta(1232)$ isobar. The corresponding results for ^{3}He and ^{3}H read

$$g_1^{^3\mathrm{He}} = \int_x^3 \frac{dy}{y} \Delta f^n_{^3\mathrm{He}}(y) g_1^n(x/y) + 2\int_x^3 \frac{dy}{y} \Delta f^p_{^3\mathrm{He}}(y) g_1^p(x/y) - 0.014(g_1^p(x) - 4g_1^n(x)), \quad (25)$$

and

$$g_1^{^3\mathrm{H}} = 2\int_x^3 \frac{dy}{y} \Delta f^n_{^3\mathrm{H}}(y) g_1^p(x/y) + \int_x^3 \frac{dy}{y} \Delta f^p_{^3\mathrm{H}}(y) g_1^n(x/y) + 0.014(g_1^p(x) - 4g_1^n(x)). \quad (26)$$

The last terms in Eqs. (25) and (26) arise from the $\Delta(1232)$ component in the ^{3}He and ^{3}H wave functions. They have sizable contributions at large values of Bjorken x, $0.2 \le x \le 0.8$.

The same formula applies for the g_2^A nuclear structure functions as

$$g_2^{^3\mathrm{He}} = \int_x^3 \frac{dy}{y} \Delta f^n_{^3\mathrm{He}}(y) g_2^n(x/y) + 2\int_x^3 \frac{dy}{y} \Delta f^p_{^3\mathrm{He}}(y) g_2^p(x/y) - 0.014(g_2^p(x) - 4g_2^n(x)) \quad (27)$$

and

$$g_2^{^3\mathrm{H}} = 2\int_x^3 \frac{dy}{y} \Delta f^n_{^3\mathrm{H}}(y) g_2^p(x/y) + \int_x^3 \frac{dy}{y} \Delta f^p_{^3\mathrm{H}}(y) g_2^n(x/y) + 0.014(g_2^p(x) - 4g_2^n(x)). \quad (28)$$

D. Shadowing and antishadowing corrections

At high energy or small values of momentum fraction x, the virtual photon can interact coherently with several nucleons in the nuclear target. This behavior is manifested in nuclear shadowing and antishadowing effects and breaks down the convolution approximation [93]. Considering these corrections, one can write the polarized nuclear structure functions as

$$g_1^{^3\mathrm{He}} = \int_x^3 \frac{dy}{y} \Delta f^n_{^3\mathrm{He}}(y) g_1^n(x/y) + 2\int_x^3 \frac{dy}{y} \Delta f^p_{^3\mathrm{He}}(y) g_1^p(x/y) - 0.014(g_1^p(x) - 4g_1^n(x)) + a(x) g_1^n(x) + b(x) g_1^p(x) \quad (29)$$

and

$$g_1^{^3\mathrm{H}} = 2\int_x^3 \frac{dy}{y}\Delta f_{^3\mathrm{H}}^n(y) g_1^p(x/y) + \int_x^3 \frac{dy}{y}\Delta f_{^3\mathrm{H}}^p(y) g_1^n(x/y) + 0.014(g_1^p(x) - 4g_1^n(x)) + a(x)g_1^n(x) + b(x)g_1^p(x). \quad (30)$$

The functions $a(x)$ and $b(x)$ describe both nuclear shadowing and antishadowing corrections and are functions of x and Q^2.

Since in the most nuclear polarized DIS experiments the x coverage does not drop below $x \sim 0.2$, the shadowing and antishadowing corrections can be ignored [61]. However, the calculations of Ref. [93] have shown that these two effects are quite significant and do affect the extraction of the nucleon spin functions at small values of Bjorken x. As mentioned earlier, current experimental data do not reach to very small values of x. Consequently, the corrections from shadowing ($10^{-4} \leq x \leq 0.03$–0.07) and antishadowing ($0.07 - 0.03 \leq x \leq 0.2$) can be completely ignored in the analysis of the present DIS data on polarized nuclei.

VI. DISCUSSION OF FIT RESULTS

The best values for parton distribution functions are demonstrated in Table II. Parameters marked with (*) are fixed after an initial minimization step to their best values. Accordingly, there are 16 unknown parameters, including the strong coupling constant, that provide enough flexibility to have a reliable fit. We achieve $\chi^2/\mathrm{dof} = 473.195/495 = 0.955$, which provides an acceptable fit to data. We extract the strong coupling constant simultaneously with polarized PDF parameters to study its correlation with the others. We obtain the value of $\alpha_s(Q_0^2) = 0.30998 \pm 0.0113$ at a 0.68% confidence level. Rescaling the coupling constant to the mass of the Z boson, we achieve $\alpha_s(M_Z^2) = 0.1106 \pm 0.0010$. The present world average value is $\alpha_s(M_Z^2) = 0.1185 \pm 0.0006$ [86].

A. Polarized parton distribution functions

Our NNLO polarized PDF along with their corresponding 0.68% C.L. uncertainties are presented in Fig. 5. Various parametrizations from the literature [9,10,53] and [45] obtained from NLO and NNLO QCD analyses of the inclusive data are presented for comparison. The

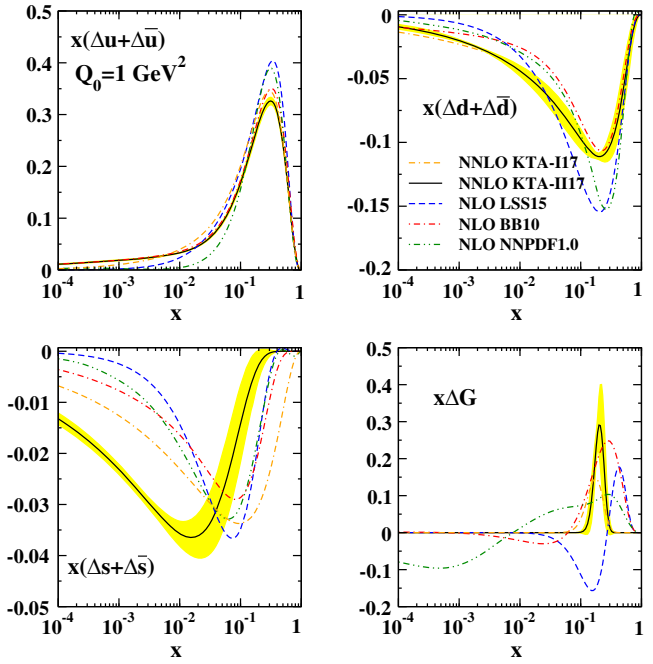

FIG. 5. Our results KTA-II17 for the polarized PDFs at $Q_0^2 = 1$ GeV^2 as a function of x in the NNLO approximation plotted as a solid curve along with their 68% C.L. uncertainties, as described in the text. We also show the results obtained in earlier global analyses of KTA-I17 (dashed-dashed-dotted) [45], LSS15 (dashed) [9], BB10 (dashed-dotted) [53], NNPDF1.0 (dashed-dotted-dotted) [10].

$x(\Delta u + \Delta\bar{u})$ and $x\Delta G$ distributions are positive, while the $x(\Delta d + \Delta\bar{d})$ and $x(\Delta s + \Delta\bar{s})$ distributions are negative.

For the $x(\Delta u + \Delta\bar{u})$ distributions, all of the curves are comparable. Examining the $x(\Delta d + \Delta\bar{d})$ distributions we see that most of the fits are in agreement, with the possible exception of the LSS15 and NNPDF1.0.

All analyses of the polarized inclusive DIS data have extracted significantly negative results for the polarized strange quark distribution functions, $x(\Delta s + \Delta\bar{s})$, for all x values, even though the parametrization allowed a sign change as a function of x.

Results for polarized gluon distribution from the various fits on the present polarized inclusive DIS data are quite spread out. The difficulties in constraining $x\Delta G$ cannot be ruled out with present data. Our gluon distribution tends to zero more quickly than the others.

TABLE II. Obtained parameter values and their statistical errors at the input scale $Q_0^2 = 1$ GeV^2 determined from leading-twist analyses in the NNLO approximation. Those marked with (*) are fixed. Note that the TMCs are included in our QCD analysis.

Flavor	η	α	β	ϵ	γ
$u + \bar{u}$	0.807^*	0.259 ± 0.007	2.857 ± 0.049	-4.95 ± 0.324	38.12 ± 1.85
$d + \bar{d}$	-0.461^*	0.332 ± 0.72	3.139 ± 0.75	0	4.53 ± 1.85
$s + \bar{s}$	-0.119 ± 0.008	0.249 ± 0.048	15.68 ± 4.21	0	0
G	0.133 ± 0.027	23.33 ± 4.32	86.57 ± 6.35	1.434 ± 0.23	-4.992 ± 0.574

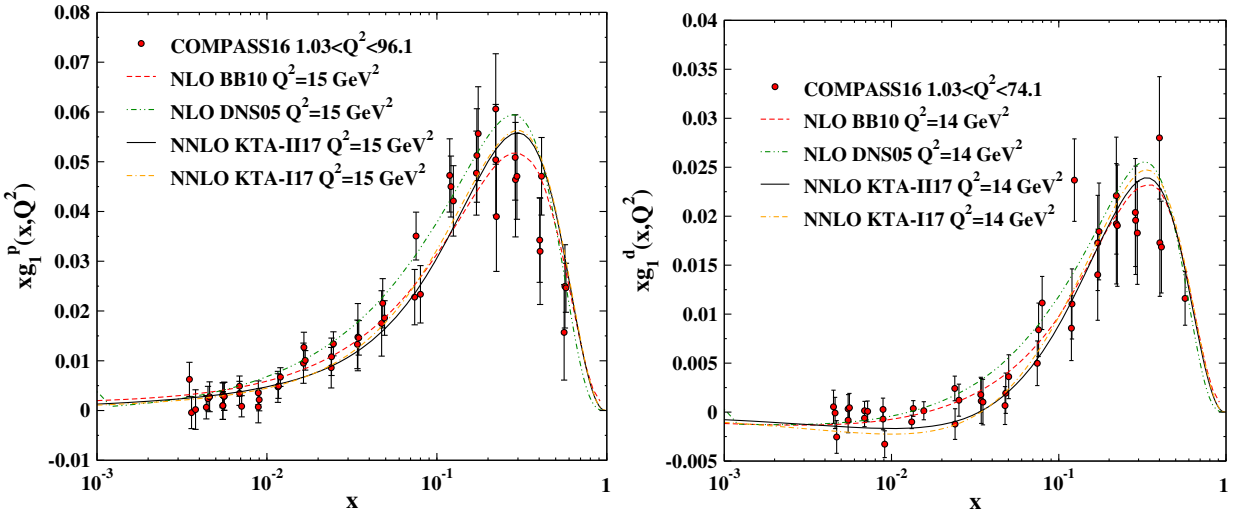

FIG. 6. KTA-II17 prediction (solid curve) for the polarized structure function of the proton (left) and deuteron (right) as a function of x for the mean value of $Q^2 = 15$ GeV^2 and $Q^2 = 14$ GeV^2, respectively. Also shown are BB10 (dashed) [53], DNS05 (dashed-dotted-dotted) [110] extracted at the NLO approximation, and KTA-I17 (dashed-dashed-dotted) [45] obtained at the NNLO approximation, together with the recent experimental data from the COMPASS16 collaborations [54,55].

B. g_1 structure functions

Figure 6 represents results for the polarized structure function xg_1^p and xg_1^d as a function of x at $Q^2 = 15$ GeV^2 and $Q^2 = 14$ GeV^2, respectively. For comparison, we illustrate the results extracted in BB10 [53], DNS05 [110] at the NLO approximation, and KTA-I17 [45] at the NNLO approximation. Our curves stay compatible with the recent COMPASS16 published data [54,55] within statistical uncertainties. Note that the experimental observables belong to the scale region of $1.03 < Q^2 < 96.1$ GeV^2 and $1.03 < Q^2 < 74.1$ GeV^2 for proton and deuteron polarized structure functions.

In Fig. 7 we present our result for the polarized structure function of neutron xg_1^n as a function of x at $Q_0^2 = 4$ GeV^2. We observe that our result coincides with those of BB10 [53], DNS05 [110] at the NLO approximation,

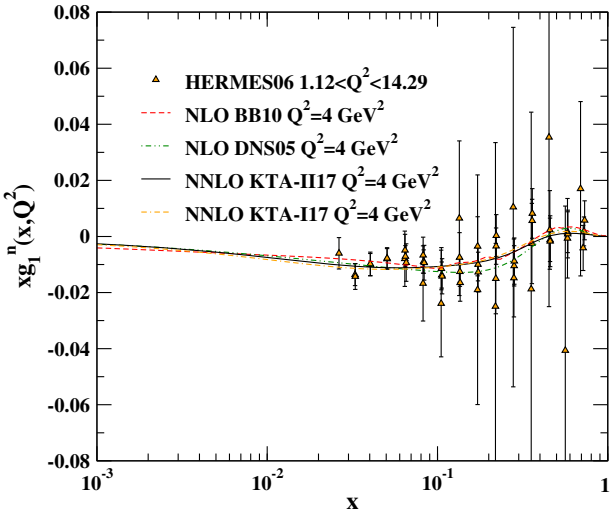

FIG. 7. KTA-II17 prediction (solid curve) for the polarized structure function of neutrons for the mean value of $Q^2 = 4$ GeV^2 as a function of x in the NNLO approximation. Also shown are BB10 (dashed) [53], DNS05 (dashed-dotted-dotted) [110] extracted at the NLO approximation, and KTA-I17 (dashed-dashed-dotted) [45] obtained at the NNLO approximation, together with the experimental data from the HERMES06 Collaboration [58].

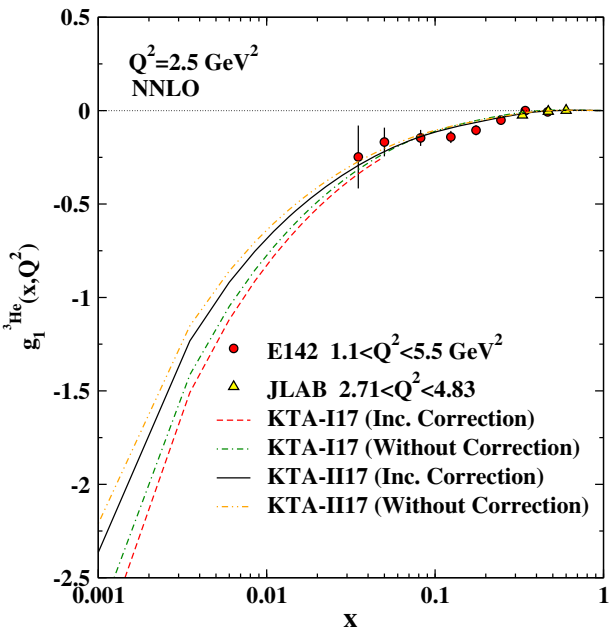

FIG. 8. Analytical results with and without nuclear corrections for the polarized structure function of $g_1^{^3\mathrm{He}}(x, Q^2)$ as a function of x at NNLO approximation. The current fit is the solid curve. Also shown are data form E142 [111] and JLAB04 [112].

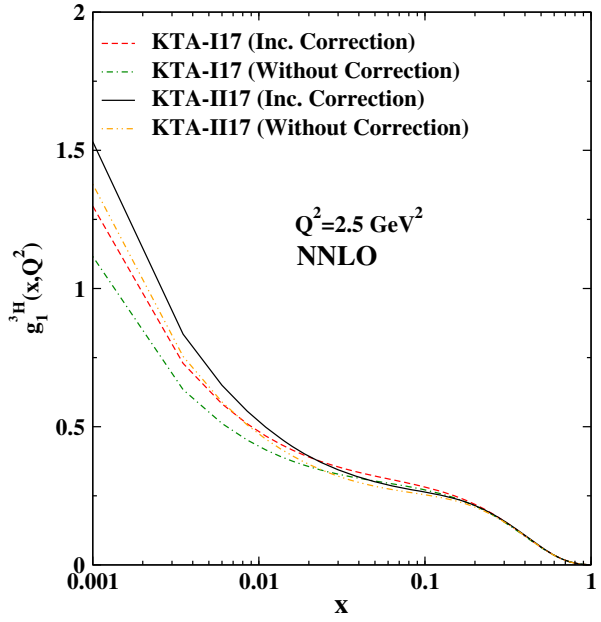

FIG. 9. Analytical results with and without nuclear corrections for the polarized structure function of $g_1^{^3\mathrm{H}}(x, Q^2)$ as a function of x at NNLO approximation. The current fit is the solid curve. Also shown are the QCD NNLO curves obtained by KTA-I17 [45] for comparison.

and KTA-I17 [45] at the NNLO approximation. The HERMES06 experimental data [58] are well described within errors by all the curves. The experimental observables belong to the scale region of $1.12 < Q^2 < 14.29$ GeV^2. Generally the xg_1^n data have larger uncertainties compared with the xg_1^p and xg_1^d data. More accurate experimental measurements on light nuclear targets are required to allow us to scrutinize neutron structure functions.

C. Nuclear polarized structure functions

We are in a position to apply the formalism developed in Sec. V to compute the $g_{1,2}^{^3\mathrm{He}}$ and $g_1^{^3\mathrm{H}}$ structure functions and corresponding nuclear corrections based on the extracted PPDFs. In particular, we study the impact of nuclear effects originating from the non-nucleonic degrees of freedom on the extraction of the spin structure of the ^{3}He and ^{3}H.

In Figs. 8 and 9, we show our results for the $g_1^{^3\mathrm{He}}$ and $g_1^{^3\mathrm{H}}$ polarized structure functions at NNLO approximation based on Eqs. (25) and (26), respectively, and compare with the curves based on KTA-I17 [45]. The experimental data from E142 [111] and JLAB04 [112] are well described by the fit in Fig. 8. One can conclude that our results for the $g_1^{^3\mathrm{He}}$ based on both of our spin-dependent PDFs (KTA-I17 and KTA-II17) reproduce the trend of the existing data.

We would like to stress again that the small x ($10^{-4} \leq x \leq 0.2$) effects from nuclear shadowing and antishadowing were not taken into account in the results presented in Figs. 8 and 9. At large x values, $x \geq 0.8$, all the results coincide. The nuclear corrections lead to a sizable difference in the small x values. For intermediate and low x values, including nuclear corrections underestimates the results.

In Figs. 10 and 11, our theory predictions for the polarized $g_1^{^3\mathrm{He}}(x, Q^2)$ and $g_2^{^3\mathrm{He}}(x, Q^2)$ structure functions are displayed as a function of x at NNLO approximation and compared with the recent data from the JLAB16 Collaboration [61]. The left plots correspond to $Q^2 = 4.74$ GeV^2 and the right ones correspond to $Q^2 = 5.89$ GeV^2. From Fig. 10, we can conclude that applying nuclear corrections to the spin-dependent ^{3}He structure functions decreases $g_1^{^3\mathrm{He}}(x, Q^2)$ at small values of x. We observe similar trends for $g_2^{^3\mathrm{He}}(x, Q^2)$

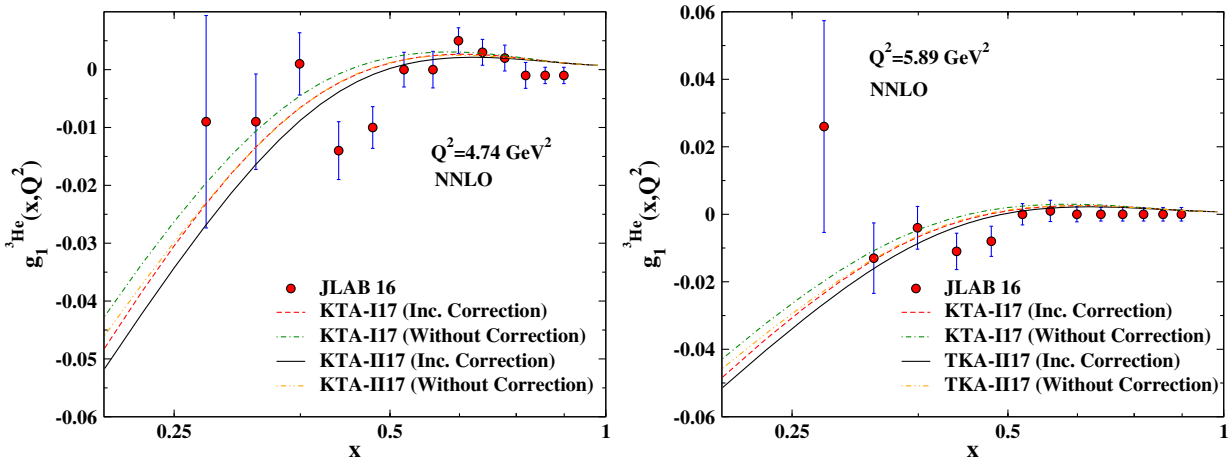

FIG. 10. Analytical result for the polarized $g_1^{^3\mathrm{He}}(x, Q^2)$ structure function as a function of x at the NNLO approximation that has been compared with the recent and up-to-date experimental data from the JLAB16 Collaboration [61]. The left plot corresponds to $Q^2 = 4.74$ GeV^2 and the right one corresponds to $Q^2 = 5.89$ GeV^2.

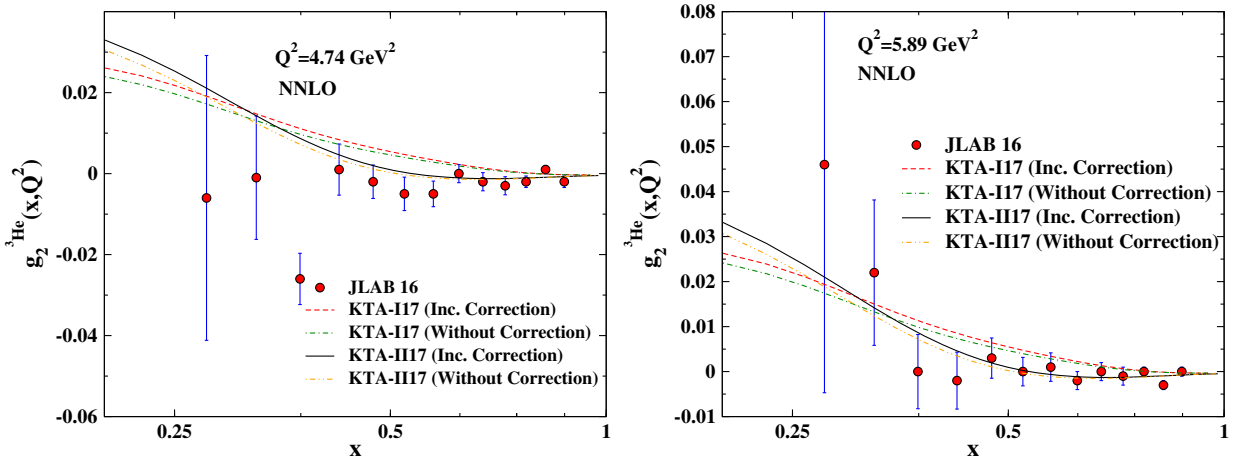

FIG. 11. Analytical result for the polarized $g_2^{^3\mathrm{He}}(x, Q^2)$ structure function as a function of x at the NNLO approximation, which has been compared with the recent and up-to-date experimental data from the JLAB16 Collaboration [61]. The left plot corresponds to $Q^2 = 4.74$ GeV^2 and the right one corresponds to $Q^2 = 5.89$ GeV^2.

in Fig. 11. Figure 11 also indicates that the results are strongly model dependent in the whole Bjorken x region. The $g_2^{^3\mathrm{He}}(x, Q^2)$ structure functions based on KTA-II17 polarized PDF describe the JLAB16 data better than KTA-I17 PPDFs.

The DIS data reported by E06-014 experiments at Jefferson Lab (JLAB) in Hall A are the latest and most up-to-date data for the spin-dependent g_1 and g_2 structure functions of ^{3}He [61]. These data sets were obtained from the scattering of a longitudinally polarized electron beam from a transversely and longitudinally polarized ^{3}He target. This measurement covers the kinematic regions of $0.25 \leq x \leq 0.9$ and 2 GeV$^2 \leq Q^2 \leq$ 6 GeV^2.

In Fig. 12, the spin-dependent $x^2 g_1^{^3\mathrm{He}}(x, Q^2)$ structure function is plotted and compared to the world DIS data from E142 [111], JLAB04 [112], JLAB03 [113], and recent data from the JLAB16 Collaboration [61]. KTA-II17 predictions follow the trend of existing data.

D. Bjorken sum rule

Having at hand the spin-dependent structure of the proton and neutron, one may also examine in more detail the Bjorken sum rule [114]

$$\int_o^1 [g_1^p(x, Q^2) - g_1^n(x, Q^2)]dx = \frac{1}{6} g_A \left[1 + \mathcal{O}\left(\frac{\alpha_s}{\pi}\right)\right], \quad (31)$$

which relates the difference of the first moments of the proton $\int_0^1 g_1^p(x, Q^2)dx$ and neutron $\int_0^1 g_1^n(x, Q^2)dx$ spin structure functions to the axial vector coupling constant measured in the β-decay of neutrons, $g_A = 1.2670 \pm 0.0035$ [86]. This sum rule can be straightforwardly generalized for the difference of the spin structure functions of ^{3}He and ^{3}H as follows [93,115]:

$$\int_0^3 [g_1^{^3\mathrm{H}}(x, Q^2) - g_1^{^3\mathrm{He}}(x, Q^2)]dx = \frac{1}{6} g_A|_{\mathrm{triton}} \left[1 + \mathcal{O}\left(\frac{\alpha_s}{\pi}\right)\right], \quad (32)$$

where $g_A|_{\mathrm{triton}}$ is the axial vector coupling constant measured in the β decay of the triton, with $g_A|_{\mathrm{triton}} = 1.211 \pm 0.002$ [116]. Finally, taking the ratio of Eqs. (31) and (32), one can find [93,115]

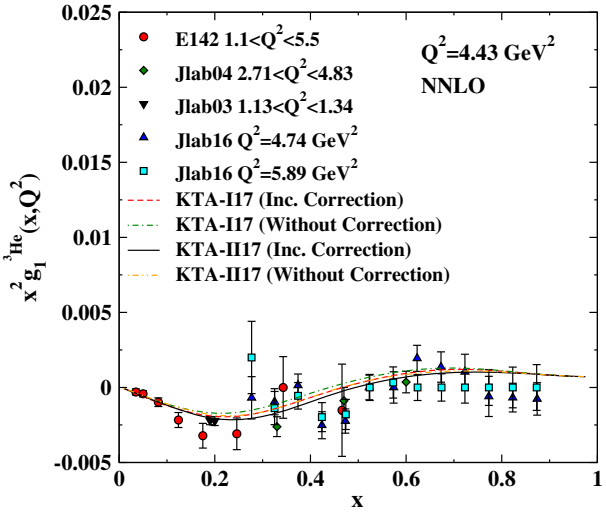

FIG. 12. KTA-II17 results for the $x^2 g_1^{^3\mathrm{He}}(x, Q^2)$ structure function as a function of x at the NNLO approximation. Our curves are compared to the world data from E142 [111], JLAB04 [112], JLAB03 [113], and recent data from the JLAB16 Collaboration [61].

$$\eta \equiv \frac{g_A|_{\text{triton}}}{g_A} = \frac{\int_0^3 [g_1^{^3\text{H}}(x,Q^2) - g_1^{^3\text{He}}(x,Q^2)]dx}{\int_0^1 [g_1^p(x,Q^2) - g_1^n(x,Q^2)]dx} = 0.9937 \pm 0.004. \quad (33)$$

We compute the above ratio to be $\eta = 0.923$ based on Eqs. (21) and (22). Including nuclear corrections [Eqs. (25) and (26)] modifies this value to $\eta = 0.970$.

One can conclude that the corrections associated with the presence of the Δ resonance change the value of the Bjorken sum rule in the $A = 3$ nuclei. It has been shown in Refs. [93,115] that the contributions to the spin-dependent structure functions of ^{3}He from non-nucleonic degrees of freedom in the nucleus, such as the $\Delta(1232)$ isobar, lead to the $\approx$4% difference between the g_A in the free nucleon and $g_A|_{\text{triton}}$ in the $A = 3$ nuclei.

VII. SUMMARY AND CONCLUSIONS

Our new NNLO analysis of the inclusive data included for the first time the extremely accurate COMPASS16 data on protons and deuterons [54,55]. During the analysis, we considered TMCs to extract the polarized PDFs inside the nucleon. We adopt more general input parametrizations for the sum of quark and antiquark polarized PDFs instead of the valence and sea quark distributions. Similar to our previous papers, we use the Jacobi polynomial method to yield the structure functions $g_1^{N=p,n,d}(x,Q^2)$ from its moments in the whole x region. Having extracted the polarized structure functions, we estimated the nuclear structure functions of $g_{1,2}^{^3\text{He}}$ and $g_1^{^3\text{H}}$.

Due to increasing levels of precision attained in new generations of polarized DIS experiments, spin-dependent ^{3}He and ^{3}H targets become essential tools for studying the spin structure of the nucleon. They are also providing the most direct means of probing the polarized quark and gluon distributions in the free neutron.

We also have performed a detailed analysis of nuclear corrections to the spin-dependent $g_{1,2}^{^3\text{He}}$ and $g_1^{^3\text{H}}$ structure functions. In addition to the corrections arising from the incoherent scattering on nuclear targets, we have examined contributions from non-nucleonic degrees of freedom and have related the strength of this correction to the Bjorken sum rule in the $A = 3$ nuclei.

In this paper, we carry out an approximate way of assessing the importance of nuclear effects. Neutron data are coming from deuterium and helium-3, and their corresponding nuclear corrections are ignored. We believe that the neutron data are only reliable if we assume nuclear effects are negligible whereas they are not. We suggest re-extracting g_1^n from $g_1^{^3\text{He}}$ data as previously argued in Ref. [93].

ACKNOWLEDGMENTS

The authors would like to thank Elliott Leader and Emanuele Nocera for their careful reading of the manuscript and helpful discussions. The authors are also grateful to the School of Particles and Accelerators, Institute for Research in Fundamental Sciences (IPM), for financial support of this project. Hamzeh Khanpour is grateful to the University of Science and Technology of Mazandaran for financial support provided for this research.

[1] R. D. Ball *et al.* (NNPDF Collaboration), Parton distributions from high-precision collider data, Eur. Phys. J. C **77**, 663 (2017).
[2] C. Bourrely and J. Soffer, New developments in the statistical approach of parton distributions: Tests and predictions up to LHC energies, Nucl. Phys. **A941**, 307 (2015).
[3] L. A. Harland-Lang, A. D. Martin, P. Motylinski, and R. S. Thorne, Parton distributions in the LHC era: MMHT 2014 PDFs, Eur. Phys. J. C **75**, 204 (2015).
[4] A. D. Martin, W. J. Stirling, R. S. Thorne, and G. Watt, Parton distributions for the LHC, Eur. Phys. J. C **63**, 189 (2009).
[5] T. J. Hou *et al.*, CT14 intrinsic charm parton distribution functions from CTEQ-TEA global analysis, arXiv:1707.00657.
[6] F. Taghavi-Shahri, H. Khanpour, S. Atashbar Tehrani, and Z. Alizadeh Yazdi, Next-to-next-to-leading order QCD analysis of spin-dependent parton distribution functions and their uncertainties: Jacobi polynomials approach, Phys. Rev. D **93**, 114024 (2016).
[7] P. Jimenez-Delgado, H. Avakian, and W. Melnitchouk (Jefferson Lab Angular Momentum (JAM) Collaboration), Constraints on spin-dependent parton distributions at large x from global QCD analysis, Phys. Lett. B **738**, 263 (2014).
[8] N. Sato, W. Melnitchouk, S. E. Kuhn, J. J. Ethier, and A. Accardi (Jefferson Lab Angular Momentum Collaboration), Iterative Monte Carlo analysis of spin-dependent parton distributions, Phys. Rev. D **93**, 074005 (2016).
[9] E. Leader, A. V. Sidorov, and D. B. Stamenov, New analysis concerning the strange quark polarization puzzle, Phys. Rev. D **91**, 054017 (2015).
[10] E. R. Nocera, R. D. Ball, S. Forte, G. Ridolfi, and J. Rojo (NNPDF Collaboration), A first unbiased global

determination of polarized PDFs and their uncertainties, Nucl. Phys. **B887**, 276 (2014).
[11] H. Khanpour and S. Atashbar Tehrani, Global analysis of nuclear parton distribution functions and their uncertainties at next-to-next-to-leading order, Phys. Rev. D **93**, 014026 (2016).
[12] K. J. Eskola, P. Paakkinen, H. Paukkunen, and C. A. Salgado, EPPS16: Nuclear parton distributions with LHC data, Eur. Phys. J. C **77**, 163 (2017).
[13] K. Kovarik *et al.*, nCTEQ15: Global analysis of nuclear parton distributions with uncertainties in the CTEQ framework, Phys. Rev. D **93**, 085037 (2016).
[14] R. Wang, X. Chen, and Q. Fu, Global study of nuclear modifications on parton distribution functions, Nucl. Phys. **B920**, 1 (2017).
[15] V. Bertone, S. Carrazza, N. P. Hartland, E. R. Nocera, and J. Rojo, A determination of the fragmentation functions of pions, kaons, and protons with faithful uncertainties, Eur. Phys. J. C **77**, 516 (2017).
[16] M. Goharipour and H. Mehraban, Predictions for the isolated prompt photon production at the LHC at $\sqrt{s} = 13$ TeV, Adv. High Energy Phys. **2017**, 3802381 (2017).
[17] H. Dahiya and M. Randhawa, Nucleon structure functions and longitudinal spin asymmetries in the chiral quark constituent model, Phys. Rev. D **93**, 114030 (2016).
[18] P. Jimenez-Delgado, A. Accardi, and W. Melnitchouk, Impact of hadronic and nuclear corrections on global analysis of spin-dependent parton distributions, Phys. Rev. D **89**, 034025 (2014).
[19] R. D. Ball, E. R. Nocera, and J. Rojo, The asymptotic behaviour of parton distributions at small and large x, Eur. Phys. J. C **76**, 383 (2016).
[20] M. Goharipour and H. Mehraban, Study of isolated prompt photon production in p-Pb collisions for the ALICE kinematics, Phys. Rev. D **95**, 054002 (2017).
[21] H. Haider, F. Zaidi, M. Sajjad Athar, S. K. Singh, and I. Ruiz Simo, Nuclear medium effects in $F_{2A}^{\mathrm{EM}}(x, Q^2)$ and $F_{2A}^{\mathrm{Weak}}(x, Q^2)$ structure functions, Nucl. Phys. **A955**, 58 (2016).
[22] A. Accardi, L. T. Brady, W. Melnitchouk, J. F. Owens, and N. Sato, Constraints on large-x parton distributions from new weak boson production and deep-inelastic scattering data, Phys. Rev. D **93**, 114017 (2016).
[23] N. Armesto, H. Paukkunen, J. M. Penín, C. A. Salgado, and P. Zurita, An analysis of the impact of LHC Run I proton–lead data on nuclear parton densities, Eur. Phys. J. C **76**, 218 (2016).
[24] L. Frankfurt, V. Guzey, M. Strikman, and M. Zhalov, Nuclear shadowing in photoproduction of ρ mesons in ultraperipheral nucleus collisions at RHIC and the LHC, Phys. Lett. B **752**, 51 (2016).
[25] L. Frankfurt, V. Guzey, and M. Strikman, Dynamical model of antishadowing of the nuclear gluon distribution, Phys. Rev. C **95**, 055208 (2017).
[26] S. M. Moosavi Nejad and P. Sartipi Yarahmadi, Heavy-quark fragmentation functions at next-to-leading perturbative QCD, Eur. Phys. J. A **52**, 315 (2016).
[27] S. M. Moosavi Nejad, M. Soleymaninia, and A. Maktoubian, Proton fragmentation functions considering finite-mass corrections, Eur. Phys. J. A **52**, 316 (2016).
[28] V. Guzey, M. Strikman, and M. Zhalov, Accessing transverse nucleon and gluon distributions in heavy nuclei using coherent vector meson photoproduction at high energies in ion ultraperipheral collisions, Phys. Rev. C **95**, 025204 (2017).
[29] H. Khanpour, M. Goharipour, and V. Guzey, Effects of next-to-leading order DGLAP evolution on generalized parton distributions of the proton and deeply virtual Compton scattering at high energy, arXiv:1708.05740.
[30] M. Salajegheh, Intrinsic strange distributions in the nucleon from the light-cone models, Phys. Rev. D **92**, 074033 (2015).
[31] N. Kalantarians, E. Christy, and C. Keppel, Comparison of the structure function F2 as measured by charged lepton and neutrino scattering from iron targets, Phys. Rev. C **96**, 032201 (2017).
[32] J. J. Ethier, N. Sato, and W. Melnitchouk, First Simultaneous Extraction of Spin-Dependent Parton Distributions and Fragmentation Functions from a Global QCD Analysis, Phys. Rev. Lett. **119**, 132001 (2017).
[33] A. Kusina, F. Lyonnet, D. B. Clark, E. Godat, T. Ježo, K. Kovařík, F. I. Olness, I. Schienbein, and J. Y. Yu, Vector boson production in proton-lead and lead-lead collisions at the LHC and its impact on nCTEQ15 PDFs, Eur. Phys. J. C **77**, 488 (2017).
[34] G. R. Boroun, Geometrical scaling behavior of the top structure functions ratio at the LHeC, Phys. Lett. B **744**, 142 (2015).
[35] G. R. Boroun, The ratio of the beauty structure functions $R^b = F_L^b/F_2^b$ at low x, Nucl. Phys. **B884**, 684 (2014).
[36] G. R. Boroun, Top structure function at the LHeC, Phys. Lett. B **741**, 197 (2015).
[37] S. Zarrin and G. R. Boroun, Solution of QCD ⊗ QED coupled DGLAP equations, Nucl. Phys. **B922**, 126 (2017).
[38] S. Atashbar Tehrani, F. Taghavi-Shahri, A. Mirjalili, and M. M. Yazdanpanah, NLO analytical solutions to the polarized parton distributions, based on the Laplace transformation, Phys. Rev. D **87**, 114012 (2013); Erratum, Phys. Rev. D **88**, 039902(E) (2013).
[39] F. Taghavi-Shahri and F. Arash, Non-singlet spin structure function in the valon model and low x scaling behavior of g_1^{NS} and g_1^p, Phys. Rev. C **82**, 035205 (2010).
[40] P. Phukan, M. Lalung, and J. K. Sarma, NNLO solution of nonlinear GLR–MQ evolution equation to determine gluon distribution function using Regge like ansatz, Nucl. Phys. **A968**, 275 (2017).
[41] M. Mottaghizadeh, F. T. Shahri, and P. Eslami, Analytical solutions of the QCD⊗QED DGLAP evolution equations based on the Mellin transform technique in NLO approximation, Phys. Lett. B **773**, 375 (2017).
[42] J. Ashman *et al.* (European Muon Collaboration), A measurement of the spin asymmetry and determination of the structure function g_1 in deep inelastic muon-proton scattering, Phys. Lett. B **206**, 364 (1988).
[43] J. Ashman *et al.* (European Muon Collaboration), An investigation of the spin structure of the proton in deep inelastic scattering of polarized muons on polarized protons, Nucl. Phys. **B328**, 1 (1989).
[44] B. Adeva *et al.* (Spin Muon Collaboration), Spin asymmetries A_1 and structure functions g_1 of the proton and

the deuteron from polarized high-energy muon scattering, Phys. Rev. D **58**, 112001 (1998).
[45] H. Khanpour, S. T. Monfared, and S. Atashbar Tehrani, Nucleon spin structure functions at NNLO in the presence of target mass corrections and higher twist effects, Phys. Rev. D **95**, 074006 (2017).
[46] H. Khanpour, A. Mirjalili, and S. Atashbar Tehrani, Analytic derivation of the next-to-leading order proton structure function $F_2^p(x, Q^2)$ based on the Laplace transformation, Phys. Rev. C **95**, 035201 (2017).
[47] C. Ayala and S. V. Mikhailov, How to perform a QCD analysis of DIS in analytic perturbation theory, Phys. Rev. D **92**, 014028 (2015).
[48] E. Leader, A. V. Sidorov, and D. B. Stamenov, NLO QCD analysis of polarized deep inelastic scattering, Int. J. Mod. Phys. A **13**, 5573 (1998).
[49] S. M. Moosavi Nejad, H. Khanpour, S. Atashbar Tehrani, and M. Mahdavi, QCD analysis of nucleon structure functions in deep-inelastic neutrino-nucleon scattering: Laplace transform and Jacobi polynomials approach, Phys. Rev. C **94**, 045201 (2016).
[50] S. Taheri Monfared, Z. Haddadi, and A. N. Khorramian, Target mass corrections and higher twist effects in polarized deep-inelastic scattering, Phys. Rev. D **89**, 074052 (2014); Erratum, Phys. Rev. D **89**, 119901(E) (2014).
[51] E. Leader, A. V. Sidorov, and D. B. Stamenov, On the role of higher twist in polarized deep inelastic scattering, Phys. Rev. D **67**, 074017 (2003).
[52] E. Leader, A. V. Sidorov, and D. B. Stamenov, Impact of CLAS and COMPASS data on polarized parton densities and higher twist, Phys. Rev. D **75**, 074027 (2007).
[53] J. Blumlein and H. Bottcher, QCD analysis of polarized deep inelastic scattering data, Nucl. Phys. **B841**, 205 (2010).
[54] C. Adolph *et al.* (COMPASS Collaboration), Final COMPASS results on the deuteron spin-dependent structure function g_1^d and the Bjorken sum rule, Phys. Lett. B **769**, 34 (2017).
[55] C. Adolph *et al.* (COMPASS Collaboration), The spin structure function g_1^p of the proton and a test of the Bjorken sum rule, Phys. Lett. B **753**, 18 (2016).
[56] K. Abe *et al.* (E143 Collaboration), Measurements of the proton and deuteron spin structure functions g_1 and g_2, Phys. Rev. D **58**, 112003 (1998).
[57] P. L. Anthony *et al.* (E155 Collaboration), Measurement of the deuteron spin structure function $g_1^d(x)$ for $1\ (\mathrm{GeV}/c)^2 < Q^2 < 40\ (\mathrm{GeV}/c)^2$, Phys. Lett. B **463**, 339 (1999).
[58] K. Ackerstaff *et al.* (HERMES Collaboration), Measurement of the neutron spin structure function g_1^n with a polarized ^{3}He internal target, Phys. Lett. B **404**, 383 (1997).
[59] K. Abe *et al.* (E154 Collaboration), Measurement of the neutron spin structure function g2(n) and asymmetry A2(n), Phys. Lett. B **404**, 377 (1997).
[60] K. Abe *et al.* (E154 Collaboration), Precision Determination of the Neutron Spin Structure Function g1(n), Phys. Rev. Lett. **79**, 26 (1997).
[61] D. Flay *et al.* (Jefferson Lab Hall A Collaboration), Measurements of d_2^n and A_1^n: Probing the neutron spin structure, Phys. Rev. D **94**, 052003 (2016).
[62] A. Airapetian *et al.* (HERMES Collaboration), Measurement of the proton spin structure function g_1^p with a pure hydrogen target, Phys. Lett. B **442**, 484 (1998).
[63] A. Airapetian *et al.* (HERMES Collaboration), Precise determination of the spin structure function g_1 of the proton, deuteron and neutron, Phys. Rev. D **75**, 012007 (2007).
[64] P. L. Anthony *et al.* (E155 Collaboration), Measurements of the Q^2 dependence of the proton and neutron spin structure functions g_1^p and g_1^n, Phys. Lett. B **493**, 19 (2000).
[65] M. G. Alekseev *et al.* (COMPASS Collaboration), The spin-dependent structure function of the proton g_1^p and a test of the bjorken sum rule, Phys. Lett. B **690**, 466 (2010); V. Y. Alexakhin *et al.* (COMPASS Collaboration), The deuteron spin-dependent structure function g_1^d and its first moment, Phys. Lett. B **647**, 8 (2007).
[66] P. L. Anthony *et al.* (E142 Collaboration), Deep inelastic scattering of polarized electrons by polarized ^{3}He and the study of the neutron spin structure, Phys. Rev. D **54**, 6620 (1996).
[67] K. Abe *et al.* (E154 Collaboration), Precision Determination of the Neutron Spin Structure Function g_1^n, Phys. Rev. Lett. **79**, 26 (1997).
[68] K. M. Kramer (Jefferson Lab E97-103 Collaboration), The search for higher twist effects in the spin-structure functions of the neutron, AIP Conf. Proc. **675**, 615 (2003).
[69] X. Zheng *et al.* (Jefferson Lab Hall A Collaboration), Precision measurement of the neutron spin asymmetries and spin-dependent structure functions in the valence quark region, Phys. Rev. C **70**, 065207 (2004).
[70] K. Kramer, D. S. Armstrong, T. D. Averett, W. Bertozzi, S. Binet, C. Butuceanu, A. Camsonne, G. D. Cates *et al.*, The Q^2-Dependence of the Neutron Spin Structure Function g_2^n at Low Q^2, Phys. Rev. Lett. **95**, 142002 (2005).
[71] E. S. Ageev *et al.* (COMPASS Collaboration), Measurement of the spin structure of the deuteron in the DIS region, Phys. Lett. B **612**, 154 (2005).
[72] V. Y. Alexakhin *et al.* (COMPASS Collaboration), The deuteron spin-dependent structure function g_1^d and its first moment, Phys. Lett. B **647**, 8 (2007).
[73] S. Moch, J. A. M. Vermaseren, and A. Vogt, The three-loop splitting functions in QCD: The helicity-dependent case, Nucl. Phys. **B889**, 351 (2014).
[74] B. Lampe and E. Reya, Spin physics and polarized structure functions, Phys. Rep. **332**, 1 (2000).
[75] E. B. Zijlstra and W. L. van Neerven, Order α_s^2 corrections to the polarized structure function $g_1(x, Q^2)$, Nucl. Phys. **B417**, 61 (1994); Erratum, Nucl. Phys. **B426**, 245 (1994); Erratum, Nucl. Phys. **B501**, 599 (1997); Erratum, Nucl. Phys. **B773**, 105 (2007).
[76] M. Lacombe, B. Loiseau, R. Vinh Mau, J. Cote, P. Pires, and R. de Tourreil, Parametrization of the deuteron wave function of the Paris n-n potential, Phys. Lett. B **101B**, 139 (1981).
[77] W. W. Buck and F. Gross, A family of relativistic deuteron wave functions, Phys. Rev. D **20**, 2361 (1979).
[78] M. J. Zuilhof and J. A. Tjon, Electromagnetic properties of the deuteron and the Bethe-Salpeter equation with one boson exchange, Phys. Rev. C **22**, 2369 (1980).

[79] S. Wandzura and F. Wilczek, Sum rules for spin dependent electroproduction: Test of relativistic constituent quarks, Phys. Lett. **72B**, 195 (1977).

[80] H. Georgi and H. D. Politzer, Freedom at moderate energies: Masses in color dynamics, Phys. Rev. D **14**, 1829 (1976).

[81] J. Blumlein and A. Tkabladze, Target mass corrections for polarized structure functions and new sum rules, Nucl. Phys. **B553**, 427 (1999).

[82] A. Piccione and G. Ridolfi, Target mass effects in polarized deep inelastic scattering, Nucl. Phys. **B513**, 301 (1998).

[83] Y. B. Dong, Target mass corrections to proton spin structure functions and quark-hadron duality, Phys. Lett. B **641**, 272 (2006).

[84] O. Nachtmann, Positivity constraints for anomalous dimensions, Nucl. Phys. **B63**, 237 (1973).

[85] S. D. Bass and A. W. Thomas, The nucleon's octet axial-charge $g_A^{(8)}$ with chiral corrections, Phys. Lett. B **684**, 216 (2010).

[86] C. Patrignani *et al.* (Particle Data Group Collaboration), Review of particle physics, Chin. Phys. C **40**, 100001 (2016).

[87] F. James and M. Roos, Minuit: A system for function minimization and analysis of the parameter errors and correlations, Comput. Phys. Commun. **10**, 343 (1975).

[88] J. Pumplin, D. Stump, R. Brock, D. Casey, J. Huston, J. Kalk, H. L. Lai, and W. K. Tung, Uncertainties of predictions from parton distribution functions. 2. The Hessian method, Phys. Rev. D **65**, 014013 (2001).

[89] A. D. Martin, R. G. Roberts, W. J. Stirling, and R. S. Thorne, Uncertainties of predictions from parton distributions. 1: Experimental errors, Eur. Phys. J. C **28**, 455 (2003).

[90] T. J. Hou *et al.*, Reconstruction of Monte Carlo replicas from Hessian parton distributions, arXiv:1607.06066.

[91] S. Shoeibi, H. Khanpour, F. Taghavi-Shahri, and K. Javidan, Determination of neutron fracture functions from a global QCD analysis of the leading neutron production at HERA, Phys. Rev. D **95**, 074011 (2017).

[92] M. Hirai, S. Kumano, and N. Saito (Asymmetry Analysis Collaboration), Determination of polarized parton distribution functions and their uncertainties, Phys. Rev. D **69**, 054021 (2004).

[93] F. R. P. Bissey, V. A. Guzey, M. Strikman, and A. W. Thomas, Complete analysis of spin structure function g_1 of ^{3}He, Phys. Rev. C **65**, 064317 (2002).

[94] V. Guzey, Nuclear shadowing in polarized DIS on LiD_6 at small x and its effect on the extraction of the deuteron spin structure function $g_1^d(x, Q^2)$, Phys. Rev. C **64**, 045201 (2001).

[95] L. Frankfurt, V. Guzey, and M. Strikman, The nuclear effects in $(g_1^{\mathrm{He}^3})$ and the Bjorken sum rule for $A = 3$, Phys. Lett. B **381**, 379 (1996).

[96] V. Guzey and M. Strikman, Nuclear effects in $g_1^A(x, Q^2)$ at small x in deep inelastic scattering on ^{7}Li and ^{3}He, Phys. Rev. C **61**, 014002 (1999).

[97] J. J. Ethier and W. Melnitchouk, Comparative study of nuclear effects in polarized electron scattering from ^{3}He, Phys. Rev. C **88**, 054001 (2013).

[98] F. R. P. Bissey, A. W. Thomas, and I. R. Afnan, Structure functions for the three nucleon system, Phys. Rev. C **64**, 024004 (2001).

[99] I. R. Afnan, F. R. P. Bissey, J. Gomez, A. T. Katramatou, S. Liuti, W. Melnitchouk, G. G. Petratos, and A. W. Thomas, Deep inelastic scattering from $A = 3$ nuclei and the neutron structure function, Phys. Rev. C **68**, 035201 (2003).

[100] G. Piller and W. Weise, Nuclear deep inelastic lepton scattering and coherence phenomena, Phys. Rep. **330**, 1 (2000).

[101] P. Fernandez de Cordoba, E. Marco, H. Muther, E. Oset, and A. Faessler, Deep inelastic lepton scattering in nuclei at $x > 1$ and the nucleon spectral function, Nucl. Phys. **A611**, 514 (1996).

[102] S. A. Kulagin, G. Piller, and W. Weise, Shadowing, binding and off-shell effects in nuclear deep inelastic scattering, Phys. Rev. C **50**, 1154 (1994).

[103] S. A. Kulagin, W. Melnitchouk, G. Piller, and W. Weise, Spin dependent nuclear structure functions: General approach with application to the deuteron, Phys. Rev. C **52**, 932 (1995).

[104] S. A. Kulagin and W. Melnitchouk, Deuteron spin structure functions in the resonance and DIS regions, Phys. Rev. C **77**, 015210 (2008).

[105] S. A. Kulagin and W. Melnitchouk, Spin structure functions of ^{3}He at finite Q^2, Phys. Rev. C **78**, 065203 (2008).

[106] S. A. Kulagin and R. Petti, Global study of nuclear structure functions, Nucl. Phys. **A765**, 126 (2006).

[107] C. Ciofi degli Atti, S. Scopetta, E. Pace, and G. Salme, Nuclear effects in deep inelastic scattering of polarized electrons off polarized ^{3}He and the neutron spin structure functions, Phys. Rev. C **48**, R968 (1993).

[108] J. L. Friar, B. F. Gibson, G. L. Payne, A. M. Bernstein, and T. E. Chupp, Neutron polarization in polarized ^{3}He targets, Phys. Rev. C **42**, 2310 (1990).

[109] T. Y. Saito, Y. Wu, S. Ishikawa, and T. Sasakawa, Triton beta decay, Phys. Lett. B **242**, 12 (1990).

[110] D. de Florian, G. A. Navarro, and R. Sassot, Sea quark and gluon polarization in the nucleon at NLO accuracy, Phys. Rev. D **71**, 094018 (2005).

[111] P. L. Anthony *et al.* (E142 Collaboration), Deep inelastic scattering of polarized electrons by polarized ^{3}He and the study of the neutron spin structure, Phys. Rev. D **54**, 6620 (1996).

[112] X. Zheng *et al.* (Jefferson Lab Hall A Collaboration), Precision measurement of the neutron spin asymmetries and spin-dependent structure functions in the valence quark region, Phys. Rev. C **70**, 065207 (2004).

[113] K. Kramer, Ph.D. thesis, College of William and Mary, 2003.

[114] J. D. Bjorken, Applications of the chiral $U(6) \otimes U(6)$ algebra of current densities, Phys. Rev. **148**, 1467 (1966).

[115] C. Boros, V. A. Guzey, M. Strikman, and A. W. Thomas, Role of the Delta (1232) in DIS on polarized ^{3}He and extraction of the neutron spin structure function $g_1^n(x, Q^2)$, Phys. Rev. D **64**, 014025 (2001).

[116] B. Budick, J. S. Chen, and H. Lin, Halflife of Molecular Tritium and the Axial Vector Interaction in Tritium Beta Decay, Phys. Rev. Lett. **67**, 2630 (1991).